Atomistic simulation of size-dependent heat capacity of liquid in molecular scale confinement at different temperatures

Rifat Mahmud[1,2] ✉, *A.K.M. Monjur Morshed*[1], *Titan C. Paul*[3]

[1]*Department of Mechanical Engineering, Bangladesh University of Engineering and Technology, Dhaka 1000, Bangladesh*
[2]*Department of Mechanical Science and Engineering, University of Illinois at Urbana-Champaign, IL 61820, USA*
[3]*Department of Mathematical Science and Engineering, University of South Carolina Aiken, Aiken, SC 29801, USA*
✉ *E-mail: rifat08@me.buet.ac.bd*

Published in Micro & Nano Letters; Received on 10th June 2018; Revised on 6th January 2019; Accepted on 29th January 2019

An enhancement of heat capacity (C_v) of nanoconfined liquid is reported using equilibrium molecular dynamics simulations using Lennard–Jones type solid–liquid molecular model. Liquid molecules are confined in between two solid surfaces with separation distance varying from 0.6 to 17.55 nm and temperature 100 K to 140 K. The obtained heat capacity of the bulk liquid is in excellent agreement with the published literature. However, in case of nanoconfined liquid, for a particular temperature and gap thickness band, a significant enhancement of heat capacity results in. For 100 K temperature and a gap thickness of 4 nm, the obtained molar heat capacity of the nanoconfined liquid is 46.45 J/mol K, i.e. the heat capacity is enhanced by 133% compared to its bulk counterpart (19.95 J/mol K). However, this broad maximum value of heat capacity shifts to a lower value at a higher temperature. At 120 and 140 K, the maximum heat capacity becomes 29.56 and 26.97 J/mol.K and the enhancement becomes 51% and 40%, respectively. The enhancement of heat capacity is attributed to the variation in density distribution, ballistic transport of thermal phonons, reduced molecular motion and a larger contribution of interfacial thermal resistance.

1. Introduction: Liquid molecules confined in the interspatial region act differently than they are in the bulk due to the small length scale and large specific surface area [1]. Such fluids have ample usage in several natural processes and industrial applications, ranging from cellular behaviour and hydration forces in biology and colloid science [2] to microelectronic devices, nanolithography and ionic liquid-based supercapacitors [3]. Consequently, understanding the thermodynamic properties and phase behaviour of such a nanoscale confined liquid has driven significant research interest recently. However, still, there is no well-developed theory that can explain these unique behaviours of fluids in molecular scale confinement [4]. However, numerous experiments and molecular simulations have been performed to study the behaviour of fluids under such nanoscale confinements [5].

Size-dependent thermodynamic properties of the confined liquid at different temperatures were reported earlier. Morshed *et al.* [6] reported a reduction in thermal conductivity of liquid argon trapped between solid copper walls at different temperatures. They reported an increase in thermal resistance of the confined liquid due to a decrease in gap thickness. Similar behaviour of liquid argon entrapped between silver solid particles was reported by Liang and Tsai [7]. They attributed it to the change in thermal resistance of the nanoconfined liquid. Earlier, Landry and McGaughey [8] also reported a change in thermal resistance for a particular range of film thickness of the confined semiconductor thin films. They found a rapid increase in thermal resistance with increasing film thickness when the film thickness is <2 nm. For liquid argon entrapped in solid copper walls, Wang *et al.* [9] reported that increasing the separation distance, thermal boundary increases initially and then approaches to a constant value asymptotically.

Klein and Kumacheva [10] documented an increase of seven orders of magnitude in effective viscosity of a simple model liquid between two parallel surfaces separated by a distance of six molecular layers. Leng [11] mentioned a 5–16 times increment of the viscosity of water under subnanometre confinement. As viscosity is related to heat capacity via Prandtl number, a qualitative and quantitative change is expected for the heat capacity of liquid under nanoscale confinement.

Previously, experimental studies revealed that the heat capacity of clusters having atoms comparable to their surface and bulk atoms deviate from that of the large systems for a specific range of temperature [2]. A traditional Einstein–Debye phonon model, which relates the heat capacity of solids to the bulk atomic vibrations cannot explain this enhancement in the heat capacity of the nanoclusters. Incorporating the contribution of surface-free energy, Avramov and Michailov [2] extended Einstein's model for the heat capacity of solids to nanoclusters. They elucidated this enhancement in heat capacity as the size- and temperature-dependent behaviour of nanoclusters [2].

Not only nanoclusters but also water confined in nanopores shows enhanced heat capacity compared to its bulk counterpart. Tombari *et al.* [12] reported an asymptotically increase in heat capacity of water entrapped in nanopores. Using temperature-modulated calorimetry in Vycor's 2 nm radius pores, they showed that at 358 K, the heat capacity of confined water increases about 1.4 times the heat capacity of bulk water. Their works suggest that for wider nanopores, the heat capacity of the confined water approaches that of the bulk water, thus indicating the size-dependent behaviour of entrapped water molecules.

Along with water, extensive works on size-dependent enhancement of heat capacity of other liquids were also reported. With precise adiabatic calorimetry measurements, Nagoe *et al.* [13] revealed anomalous behaviour of heat capacity and density of benzene in silica Mobil Composition of Matter No. 41 (MCM-41) mesopore having an average diameter equal to and smaller than 2.9 nm. For 0–300 K temperature, an enhanced heat capacity of hydrogen inside a norbornene-based aerogel has been recently reported by the experimental works of Kucheyev and Lenhardt [14]. Cleve *et al.* revealed the size and thermal effect on the effective heat capacity of hydrogen and deuterium entrapped in silica-aerogel [15]. However, none of the earlier researchers investigated the size dependency of the heat capacity of liquid argon under nanoscale confinement at different temperatures.

In this research work, the constant volume heat capacity (C_v) of a simplified liquid (Ar) for various confinement sizes at different temperatures has been evaluated using equilibrium molecular dynamics (EMD) simulations. At first, the heat capacity of the bulk liquid has

doi: 10.1049/mnl.2018.5288

been evaluated and then the heat capacity of the confined liquid has been determined. The obtained heat capacity of the bulk liquid has been validated with the available data from the literature and National Institute of Standards and Technology (NIST). The findings of this research posit fundamental understandings on the heat capacity of the nanoconfined liquid that can find its usage in a pressurised cell with entrapped molecular species subjected to different temperature environments, and provide guidance for real world applications including the design of nanoconfined reactive cells and nanodevices.

2. Molecular simulation procedures: The molecular system adopted for this study contains a thin film of liquid sandwiched between solid walls with a few nanometre gap thickness. This gap thickness is varied from 0.6 to 17.55 nm. The top and bottom of the $6.50 \times h \times 6.50\,\text{nm}^3$ simulation box consist of three layers of solid copper (Cu) walls as shown in Fig. 1. The lattice structure is face-centred cubic (100) and the initial temperature of the simulation domain is set to be 100 K. The density of Cu atoms is 8960 kg/m^3 with 698 atoms at each layer. Liquid Ar molecules with a density of 1320 kg/m^2 are placed in between the solid Cu walls.

Using the simplified Lennard–Jones (LJ) model, the atom to atom interaction has been estimated. Van der Waal's interactions between liquid–liquid, liquid–solid and solid–solid molecules were modelled using LJ 6–12 potential using a cut-off distance of 3.5a. The standard LJ pair potential used for the simulation is [16]

$$\phi_{\text{truncated}}(r_{ij}) = 4\epsilon\left[\left(\left(\frac{\sigma}{r_{ij}}\right)^{12} - \left(\frac{\sigma}{r_{ij}}\right)^{6}\right) - \left(\left(\frac{\sigma}{r_c}\right)^{12} - \left(\frac{\sigma}{r_c}\right)^{6}\right)\right], \tag{1}$$

where 'r_{ij}' is the intermolecular distance, 'ϵ' is the depth of the potential well, 'σ' is the finite distance at which the inter-particle potential is zero, and 'r_c' is the cut-off radius.

The length and energy parameters of the interaction potential are presented in Table 1 which was collected from [17].

The Lorentz–Berthelot mixing rule was employed to calculate the intermolecular distance and depth of the potential well for solid–liquid interactions [16]

$$\sigma_{ij} = \frac{\sigma_{ii} + \sigma_{jj}}{2}, \tag{2}$$

$$\epsilon_{ij} = \sqrt{\epsilon_{ii}\epsilon_{jj}}. \tag{3}$$

Time integration is done using the velocity-Verlet algorithm using 3 fs time step. Boundary conditions (x and z) at the lateral directions are periodic while the rest one is fixed.

To avoid the drifting of solid molecules, only the bottommost and topmost layers are allowed to vibrate applying each molecule a spring force of 57 σ/ϵ^2. The adjacent solid layers are used as the thermal bath. Nose–Hoover thermostat was used to control the temperature of the solid wall. The simulation was run for 1 ns from its initial configuration turning the Nose–Hoover thermostat at 100 K. After that for 1 ns, it is kept on switching off the entire thermostat (relaxation period). At the end of this period, the time and spatial average of the total energy and the temperature of the liquid region are evaluated when the simulation reached its equilibrium state.

C_v of the bulk liquid is evaluated using the fluctuation formula that comes from statistical thermodynamics [16]:

$$C_v = \frac{\text{var}(E_T)}{K_B T^2} = \frac{\sigma^2(E_T)}{K_B T^2}, \tag{4}$$

where 'E_T' is the total energy, 'K_B' is the Boltzman constant and 'T' is the average temperature of the system.

For a constant temperature and pressure, in the confined liquid, phonon mean-free path 'l' is determined with the following equation [18]:

$$l = \frac{\bar{v}}{z} = \frac{K_B T}{\sqrt{2}\sigma p} = \frac{K_B T}{\sqrt{2}(\pi d^2) p}, \tag{5}$$

where 'T' is the average temperature of the liquid, 'd' is the collision diameter of liquid Ar molecules and 'p' is the average pressure of the liquid. The standard values of collision diameter, 'd' for liquid Ar was taken to be 0.33 nm [18] and collision cross section, 'σ' was 0.342 nm^2 [18].

The simulation was first run with an initial gap thickness to lattice spacing ratio (h/a) of 1.0. After completion, the entire procedure was repeated for higher values of h/a (up to 30.0) for 100 K. Simulations were also performed for two other temperatures (120 and 140 K) considering the fact that critical temperature and pressure of Ar are 150.687 K and 4.8630 MPa, respectively [19]. All the simulations are carried out using LAMMPS [20], visualisation is performed with OVITO [21]

3. Results and discussions: In order to explore the fluctuation thermodynamic properties of liquid Ar, all the simulations were run in canonical ensemble initially for the longer time scale. Meanwhile, in this relaxation period, temperature and total energy of the liquid system were continuously observed to ensure whether the equilibrium state was reached (Fig. 2).

The phase of the material dictates its heat retaining capability. Hence, after the equilibration, pressure and temperature of the fluid, for both bulk and liquid cases, were monitored to make

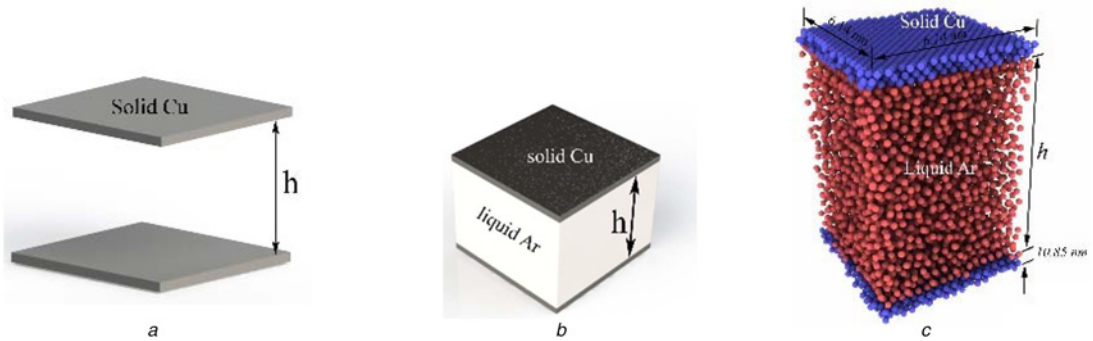

Fig. 1 *Liquid Ar in molecular scale confinement by solid Cu walls*
a Schematic without liquid Ar
b Schematic with liquid Ar
c Atomistic view of the model

sure that the fluid was liquid throughout the simulation time domain (Fig. 3).

3.1. Heat capacity-bulk liquid

3.1.1. Thickness and temperature dependence: C_v of the bulk liquid was evaluated using two different methods – fluctuation formula and centred finite difference technique (t/c) and compared with NIST database for liquid Ar [20] as shown in Fig. 4. As the fluctuation formula for both cases matched closely to the experimental values, it was adopted to evaluate the heat capacity of nanoconfined liquid whose data is not readily available.

3.2. Heat capacity-nanogap confined liquid

3.2.1. Effect of gap thickness: The change in heat capacity of the confined liquid with the variation of gap thickness is presented in Fig. 5 for a temperature of 100 K. As can be seen from Fig. 5, from $h/a = 1.5$ to $h/a = 10.5$ ('a' is the lattice constant of liquid Ar), i.e. from 0.88 to 6.14 nm, C_v of the confined liquid is higher than the bulk liquid at the same temperature. When the gap thickness is <10.5a, C_v starts to increase with the decrease gap thickness, reaches a peak value of about 46.45 J/mol K at a gap thickness of 7a (4 nm), and becomes slightly less than the bulk liquid when the gap thickness decreases to a value beyond 1.5a (0.88 nm). This maximum value of heat capacity (46.45 J/mol K) shows a 133% enhancement in heat capacity compared to that of the bulk liquid Ar (19.95 J/mol K) due to the effect of confinement.

In general, the total number of available degrees of freedom (DOFs) contributes to the heat capacity of a confined liquid [18]. Thermal energy is thought to be stored in these DOFs [18]. This stored energy can be in the form of translational kinetic energy, rotational kinetic energy or some other forms such as potential energy in vibrational modes. Consequently, as the number of available DOFs increases, heat retaining capacity of the material also increases [18]. According to this hypothesis, for monatomic gases such as helium, neon, and argon, C_v is $1/2R \times 3 = 3/2R = 12.4717$ J/mol K since for any individual atom of a monatomic gas only three DOFs contributes to its thermal energy [23]. However, the value of C_v becomes $5/2 \times R = 20.79$ J/mol K for monatomic liquid, which indicates the presence of five active DOFs in monatomic liquid [23].

Although the heat capacity of solids can be predicted using existing theories, there is no such straightforward theory that can give an accurate prediction of the heat capacity of liquids [23]. However, after the Brillouin scattering experiments by Yakov Frenkel [24], which ensures the existence of transverse phonons in liquids, a theoretical foundation to explain the heat capacity of the liquid has been established [24]. The heat capacity of simple liquids can be well approximated using the modified Debye model on this basis [24]. However, for nanoconfined liquid, modified Debye model fails to predict its heat capacity [13]. The anomalous behaviour of heat capacity of the nanoconfined liquid obtained experimentally and through simulation is attributed to some of its key aspects such as (i) non-uniformity in the distribution of liquid molecules' density; (ii) enhanced contribution of ballistic phonon transmission; (iii) reduction in molecular motion for the thermal energy transportation; and (iv) increased contribution of interfacial thermal resistance [25].

The number density profile shown in Fig. 6a illustrates the non-uniformity in the distribution of liquid molecules. From the figure, it is evident that the liquid domain consists of three distinct regions. Valiant oscillation in the density of the liquid is observed near both the solid walls. Approximately after 2 nm of this density oscillation from each solid Cu wall, the density layering of liquid Ar seems to be neutralised and becomes stable. Strong solid–liquid interactions compared to weaker liquid–liquid interactions are the key factor for this density oscillation [14]. Near the wall, liquid molecules are packed as if they were immobile solid molecules and denoted as 'solid-like-liquid' region as seen from Fig. 6b. With lower mobility and higher average density, this layer acts as a barrier to the transportation of thermal energy. Moreover, as the total number of

Table 1 LJ interaction parameters

Pair interaction	$\epsilon_{ij}(J)$	σ_{ij}(nm)
liquid–liquid	1.67 × 10−21	0.3405
solid–solid	6.59 × 10−20	0.234

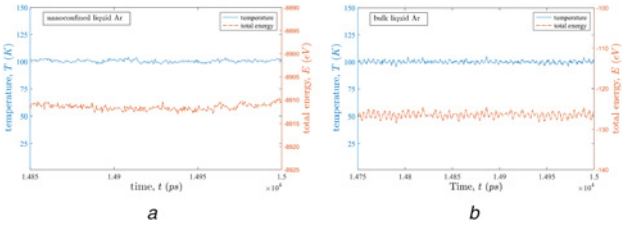

Fig. 2 *Variation of total energy and temperature in the relaxation period ($h/a = 8.5$, i.e. for a gap thickness of 5 nm)*
a Nanoconfined Ar
b Bulk Ar

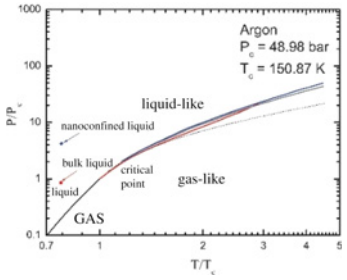

Fig. 3 *Reduced phase diagram of Ar [22]*

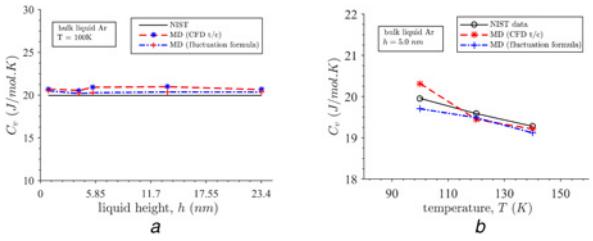

Fig. 4 *Heat capacity of the bulk liquid Ar*
a For a different height of the liquid
b For different temperature

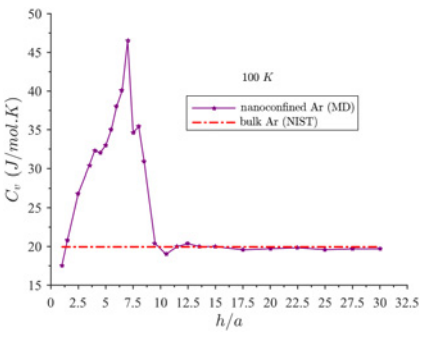

Fig. 5 *Enhancement of heat capacity at 100 K for a specific gap thickness band*

doi: 10.1049/mnl.2018.5288

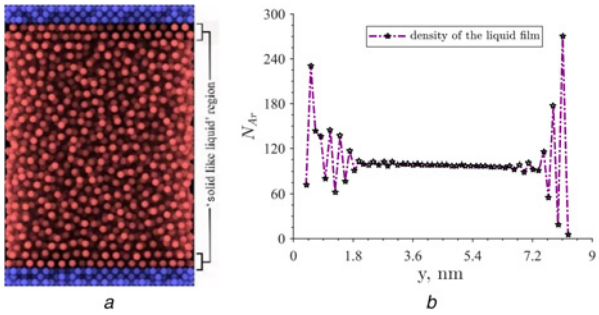

Fig. 6 *Nonuniform distribution of nanoconfined liquid*
a Number density profile of entrapped liquid
b Fluctuation of liquid's density near the confinement walls (film thickness 5.0 nm and temperature 100 K)

liquid Ar molecules is constant, an increase in density in the 'solid-like-liquid' layer indicates a reduction of molecules in the 'liquid region' which are actually the carriers of thermal energy. Hence, C_v increases as soon as the 'solid-like-liquid' layer forms.

Transmission behaviour of thermal phonons changes with the change of gap thickness. When the gap thickness is considerably larger than the Mean Free Paths (MFPs) of thermal phonons, phonons get more chance to be scattered and that is why phonon transmission is purely diffusive in this case [26]. Also, for the diffusive phonon transmission, total thermal resistance equals the sum of the thermal resistance offered by the fluid, the interface between the solid and liquid, and the thermal resistance of the liquid [26], i.e. it follows the thermal circuit model. C_v of the confined liquid, in such a case, approximates that of its bulk counterpart as shown in Fig. 5 for a higher gap thickness ($h/a > 10.5$).

However, as soon as the gap thickness becomes comparable to phonon MFPs, the transmission pattern of thermal phonon shifts from diffusive to ballistic [8] and coherent transport [3, 27]. The calculated phonon MFPs at 100 K is around 6 nm and the enhancement in C_v starts as soon as h/a drops below 10.5, i.e. gap thickness reduces below 6.14 nm, which supports the aforementioned hypothesis. For such thin films, Umklapp scattering becomes the dominating scattering mechanism of thermal phonon [26] allowing low phonon transmission and increasing the heat retaining capacity of the entrapped liquid.

However, a further decrease in gap thickness causes the suppression of long wavelength propagation of thermal phonons and the transmission becomes transient ballistic and diffusive as studied by Majumder and Joshi earlier [28]. Such a transient mode of phonon transmission is associated with reduced frequency, i.e. a larger phonon MFP [26], which ultimately associated with higher transmission of thermal phonons. That is the reason why C_v drops after reaching its peak value as seen from Fig. 5.

Mode of energy transfer in a fluid dictates molecular mobility to a great extent. For a fluid, (7) governs the heat flux (J_y) [29]

$$J_y = \frac{1}{V}\left[\sum_i \left(\frac{1}{2}mv_i^2 + \phi_i\right)v_{i,y} + \frac{1}{2}\sum_i \sum_{j>i}\left[F_{ij}\left(v_i + v_j\right)\right]y_{ij}\right]. \quad (6)$$

The first part of this equation indicates energy transfer due to molecular motion and the second part denotes energy transfer due to molecular interaction. Although for liquid, the majority of thermal energy is transmitted through molecular interaction; when the gap thickness decreases, the contribution of molecular motion becomes prominent as presented in Fig. 7*a*. To figure out the contribution of molecular motion, the self-diffusion coefficient is determined using (8) for different gap thickness

$$D = \lim_{t\to\infty} \sum_{i=1,N} \left(\left|r_i(t) - r_i(0)\right|^2\right). \quad (7)$$

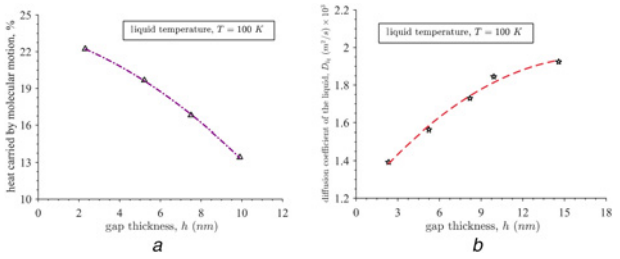

Fig. 7 *Effect of confinement size on molecular motion and molecular diffusion*
a Decrease in molecular mobility with the increase in gap thickness
b Decrease in molecular diffusion with the decrease in gap thickness

From Fig. 7*b* it is evident that the self-diffusion coefficient decreases with the reduction of gap thickness. Reduction in heat diffusion capability paves the way to an increase heat retaining capability as the gap thickness decreases and becomes comparable to phonon MFPs.

Interface thermal resistance (ITR), for confined liquid, plays an important role in the enhancement of its heat capacity. Although ITR depends on the interaction strength between solid and liquid molecules and temperature at the interface, it does not depend on the liquid film thickness [14]. As a result, ITR influences more on the overall thermal resistance with the decrease of gap thickness increasing the thermal resistance of the system which in turns increases its heat retaining capability.

Depending on confinement height, the direction of the molecules' motion varies. Confinement reduces chaotic to and fro motion of the bulk liquid molecule to a definite ordered path (Figs. 8*a* and *b*). As irregular disordered movement is more favourable to the transportation of heat, a guided motion imposes a restriction in the transportation of heat. This, eventually, enhances the heat capacity when the confinement effect comes into being.

All these facts simultaneously affect each other, resulting in an enhancement of C_v of the confined liquid for a particular range of gap thickness at a fixed temperature as shown in Fig. 5.

3.2.2. Temperature dependence of heat capacity: The change of heat capacity of the confined liquid with the change in gap thickness was extended for temperature variations (120 and 140 K). For all the three cases (100, 120 and 140 K), a significant shift in heat capacity is observed but its magnitude strongly depends on temperature.

As can be observed from Fig. 9*c*, C_v starts to increase as h/a goes beyond 10.5, 6.0 and 5.5, and reaches its maximum value at $h/a = 7.0$, 4.5 and 3.5 for $T = 100$, 120 and 140 K, respectively. The results indicate that the more the temperature of the confined liquid, the narrower the h/a band where significant fluctuation of heat capacity occurs and the lower the value of maximum heat capacity. However, one thing that is common to all these three cases is that at $h/a = 1.5$, i.e. at a gap thickness of 0.88 nm, the enhancement of heat capacity due to confinement vanishes. Moreover, when $h/a < 1.5$, i.e. when the gap thickness falls below 0.88 nm, C_v of the confined liquid becomes slightly lower than the bulk liquid. This was explained by Wang *et al.* [9], Cui *et al.* [30] and Liang and Tsai [26] earlier as the thermal boundary resistance becomes one magnitude smaller compared to larger gap thickness when the confinement contains only one atomic nanolayer.

Fig. 9*d* presents these phenomena more pronouncedly where heat capacity is normalised by dividing it with the corresponding bulk value and gap thickness is normalised by dividing it with $h/a = 10.5$. Another significant observation from Figs. 9*c* and *d* is that although the band thickness and peak value of heat capacity are dependent on temperature, in all cases the slope of the increasing and decreasing portions of the curves are analogous, which

depicts that the change of heat capacity with respect to gap thickness is independent of temperature for nanogap confined liquid up to the corresponding critical value of h/a, i.e. $(h/a)^*$. Moreover, the maximum value of heat capacity falls to a lower value as the temperature increases. As seen from Figs. 5, 9*a* and *b*, the maximum values of the heat capacity for 100, 120 and 140 K temperature are 46.45, 29.56 and 26.97 J/mol K, respectively, whereas heat capacity of the bulk liquid Ar at corresponding temperatures are 19.95, 19.58 and 19.27 J/mol K, respectively. The size-dependent heat capacity of nanoconfined liquid at different temperatures has also been reported earlier [12, 31, 32].

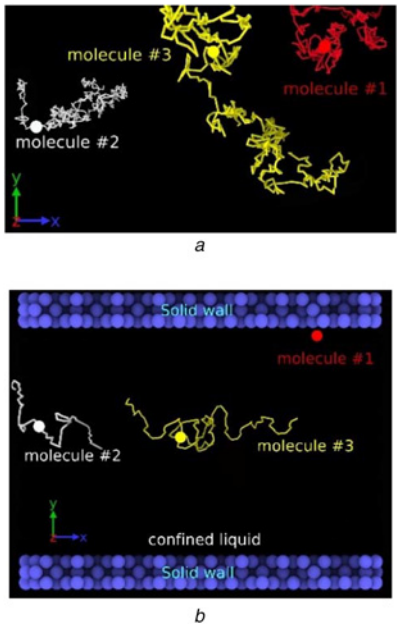

Fig. 8 *Trajectory of three predefined liquid molecules for a time period of 0.1 ns (1000 frames) at 100 K*
a Bulk liquid Ar
b Nanoconfined liquid Ar

At higher temperatures, thermal transport is provided by phonons with lesser frequencies [26]. This results in higher phonon transport [26]. Eventually, thermal transport becomes smoother resulting in low heat capacity as the temperature increases.

The variation of wall surface temperature, i.e. liquid temperature affects the density variation, but still, near the wall, vigorous oscillation of the liquid molecules remains almost unaltered. As seen from Fig. 10*a*, at a higher temperature density fluctuation, relaxed quickly. However, in the first few layers near the solid walls, there is almost no change in the number density of liquid molecules. Consequently, at higher temperatures, the number density of liquid molecules increases in between the solid walls as seen in Fig. 10*b* which implies an increase of thermal transport as the temperature increases, decreasing its heat retaining capability.

Moreover, although the liquid molecules near the solid wall do not move, the mobility of the far-wall liquid molecules, which is guided by the solid wall as shown in Fig. 8*b* increases due to the increase in temperature. Enhanced guided molecular mobility dictates a larger amount of thermal transport (7) decreasing heat retaining capability.

4. Conclusions: In summary, using classical EMD, the constant volume molar heat capacity (C_v) of liquid in molecular scale confinement at different temperatures has been investigated. To study the effect of variation of gap thickness on heat capacity at various temperatures of such nanoconfined liquid is the main focus of this investigation. The simulation results lead to the following conclusions:

(i) The liquid in molecular scale confinement exhibits enhanced heat capacity than the bulk for a specific gap thickness band, which strongly depends on the temperature of the confined liquid. Beyond this, its heat capacity resembles that of the bulk liquid.

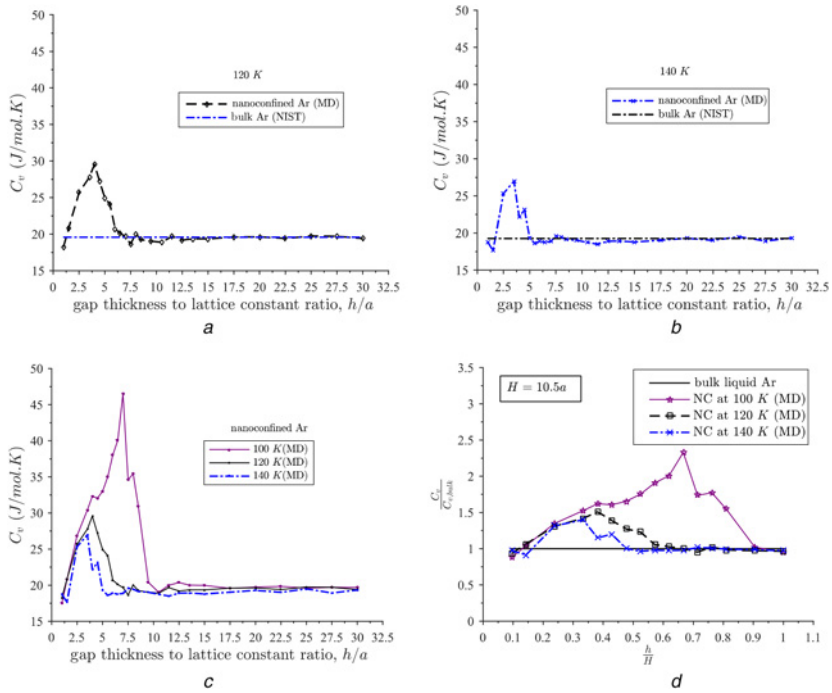

Fig. 9 *Variation of heat capacity with confinement height at different temperatures of the liquid*
a For 120 K
b For 140 K
c For all three cases (100, 120, 140 K)
d Normalised

doi: 10.1049/mnl.2018.5288

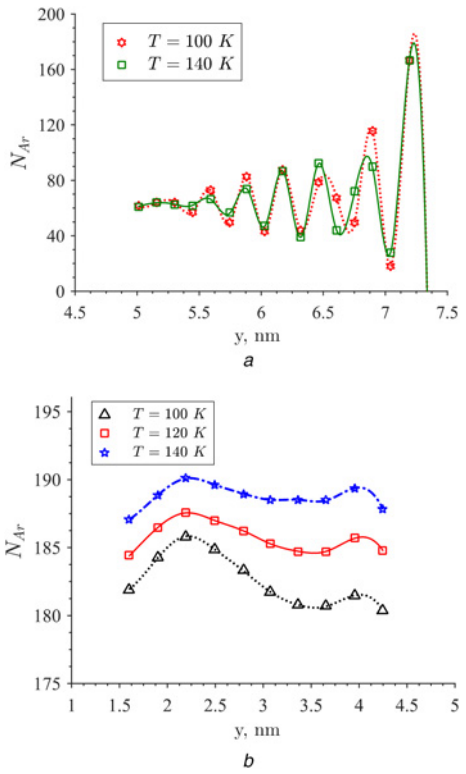

Fig. 10 *Density oscillation at different temperatures*
a Near the wall
b In liquid

(ii) The more the temperature of the confined liquid, the narrower the gap thickness band where this significant shift in heat capacity occurs.

(iii) As the temperature of the confined liquid increases, the value of the maximum heat capacity also decreases sharply. Here, as the temperature increases from 100 to 140 K, maximum heat capacity falls from 46.45 to 26.97 J/mol K.

(iv) Depending upon the temperature, for a particular gap thickness, the maximum heat capacity of the confined liquid can be as high as more than double than that of the bulk liquid (enhancement around 133%).

(v) Change in the pattern of the density distributions, ballistic phonon transport, drastic reduction in molecular motion and a sharp increase in interfacial thermal resistance on the overall thermal resistance is identified as the causes of the enhancement of heat capacity of the nanogap confined liquid.

5 References

[1] Chen X., Cao G., Han A., *ET AL.*: 'Nanoscale fluid transport: size and rate effects', *Nano Lett.*, 2008, **8**, (9), pp. 2988–2992
[2] Avramov I., Michailov M.: 'Specific heat of nanocrystals', *J. Phys., Condens. Matter*, 2008, **20**, (29), p. 295224
[3] Wang Y., Huang H., Ruan X.: 'Decomposition of coherent and incoherent phonon conduction in superlattices and random multilayers', *Phys. Rev. B*, 2014, **90**, (16), p. 165406
[4] Bolmatov D., Brazhkin V.V., Trachenko K.: 'The phonon theory of liquid thermodynamics', *Sci. Rep.*, 2012, **2**, p. 421. Available at https://doi.org/10.1038/srep00421, accessed 11 March 2017.
[5] Gai L., Iacovella C.R., Wan L., *ET AL.*: 'Examination of the phase transition behavior of nano-confined fluids by statistical temperature molecular dynamics', *J. Chem. Phys.*, 2015, **143**, (5), p. 054504
[6] Morshed A.K.M.M., Paul T.C., Khan J.A.: 'Atomistic simulation of temperature dependent thermal transport across nanoconfined liquid', *Phys. E, Low-Dimens. Syst. Nanostructures*, 2013, **47**, pp. 246–251
[7] Liang Z., Tsai H.-L.: 'Effect of molecular film thickness on thermal conduction across solid-film interfaces', *Phys. Rev. E*, 2011, **83**, (6), p. 061603
[8] Landry E.S., McGaughey A.J.: 'Effect of film thickness on the thermal resistance of confined semiconductor thin films', *J. Appl. Phys.*, 2010, **107**, (1), p. 013521
[9] Wang X., Cheng P., Quan X.: 'Molecular dynamics simulations of thermal boundary resistances in a liquid between two solid walls separated by a nano gap', *Int. Commun. Heat Mass Transf.*, 2016, **77**, pp. 183–189
[10] Klein J., Kumacheva E.: 'Confinement-induced phase transitions in simple liquids', *Science*, 1995, **269**, (5225), pp. 816–819
[11] Leng Y.: 'Hydration force and dynamic squeeze-out of hydration water under subnanometer confinement', *J. Phys., Condens. Matter*, 2008, **20**, (35), p. 354017
[12] Tombari E., Salvetti G., Ferrari C., *ET AL.*: 'Heat capacity of water in nanopores', *J. Chem. Phys.*, 2005, **123**, (21), p. 214706
[13] Nagoe A., Oguni M., Fujimori H.: 'Low-temperature heat capacities of confined liquid benzene, implying the behavior of ordinary bulk liquids', *J. Phys., Condens. Matter*, 2015, **27**, (45), p. 455103
[14] Kucheyev S.O., Lenhardt J.M.: 'Freezing hydrogen in nanoconfinement', *Fusion Sci. Technol.*, 2018, **73**, (3), pp. 1–5
[15] Van Cleve E., Worsley M.A., Kucheyev S.O.: 'Liquid–solid phase transition of hydrogen and deuterium in silica aerogel', *J. Appl. Phys.*, 2014, **116**, (16), p. 163517
[16] Allen M.P., Tildesley D.J.: 'Computer simulation of liquids' (Clarendon Press, Oxford University Press, Oxford, England, New York, 1987)
[17] Shao C., Bao H.: 'A molecular dynamics investigation of heat transfer across a disordered thin film', *Int. J. Heat Mass Transf.*, 2015, **85**, pp. 33–40
[18] Ladd M.F.C.: 'Introduction to physical chemistry' (Cambridge University Press, Cambridge, UK, 1998)
[19] 'Thermophysical properties'. Available at http://webbook.nist.gov/cgi/fluid.cgi?ID=C7440371&Action=Page, accessed 11 April 2017
[20] Plimpton S.: 'Computational limits of classical molecular dynamics simulations', *Comput. Mater. Sci.*, 1995, **4**, (4), pp. 361–364
[21] Stukowski A.: 'Visualization and analysis of atomistic simulation data with OVITO – the open visualization tool', *Model. Simul. Mater. Sci. Eng.*, 2009, **18**, (1), p. 015012
[22] Gorelli F.A., Bryk T., Krisch M., *ET AL.*: 'Dynamics and thermodynamics beyond the critical point', *Sci. Rep.*, 2013, **3**, p. 1203. Available at https://doi.org/10.1038/srep01203
[23] Wikipedia: 'Heat capacity' (Wikipedia, the free Encyclopaedia, 2017)
[24] Frenkel J.: 'Kinetic theory of liquids', vol. **8** (Dover Publisher, New York, 1955), p. 143
[25] Mahmud R., Morshed A.K.M.M., Paul T.C.: 'Heat capacity of nanoconfined liquid: a molecular dynamics simulation', p. V008T10A073, November 2017
[26] Donald R.A., Pradeep P.P., Bhattacharya D.: 'Essentials of materials science and engineering' (Cengage Learning, USA, 2013, 3rd edn.), p. 51
[27] Ravichandran J., Yadav A.K., Cheaito R., *ET AL.*: 'Crossover from incoherent to coherent phonon scattering in epitaxial oxide superlattices', *Nat. Mater.*, 2014, **13**, (2), pp. 168–172
[28] Joshi A., Majumdar A.: 'Transient ballistic and diffusive phonon heat transport in thin films', *J. Appl. Phys.*, 1993, **74**, (1), pp. 31–39
[29] Schelling P.K., Phillpot S.R., Keblinski P.: 'Comparison of atomic-level simulation methods for computing thermal conductivity', *Phys. Rev. B*, 2002, **65**, (14), p. 144306
[30] Cui W., Shen Z., Yang J., *ET AL.*: 'Molecular dynamics simulation on the microstructure of absorption layer at the liquid–solid interface in nanofluids', *Int. Commun. Heat Mass Transf.*, 2016, **71**, pp. 75–85
[31] Nagoe A., Kanke Y., Oguni M., *ET AL.*: 'Findings of C_p maximum at 233 K for the water within silica nanopores and very weak dependence of the T_{max} on the pore size', *J. Phys. Chem. B*, 2010, **114**, (44), pp. 13940–13943
[32] Mochizuki K., Koga K.: 'Solid–liquid critical behavior of water in nanopores', *Proc. Natl. Acad. Sci.*, 2015, **112**, (27), pp. 8221–8226